Environmental Science & Technology

Subscriber access provided by OCCIDENTAL COLL

Environmental Processes

Calcium-facilitated aggregation and precipitation of the uranyl peroxide nanocluster U in the presence of Na-montmorillonite

Luke R. Sadergaski, Meena Said, and Amy E. Hixon

Environ. Sci. Technol., **Just Accepted Manuscript** • DOI: 10.1021/acs.est.8b06731 • Publication Date (Web): 28 Mar 2019

Downloaded from http://pubs.acs.org on March 28, 2019

Just Accepted

“Just Accepted” manuscripts have been peer-reviewed and accepted for publication. They are posted online prior to technical editing, formatting for publication and author proofing. The American Chemical Society provides “Just Accepted” as a service to the research community to expedite the dissemination of scientific material as soon as possible after acceptance. “Just Accepted” manuscripts appear in full in PDF format accompanied by an HTML abstract. “Just Accepted” manuscripts have been fully peer reviewed, but should not be considered the official version of record. They are citable by the Digital Object Identifier (DOI®). “Just Accepted” is an optional service offered to authors. Therefore, the “Just Accepted” Web site may not include all articles that will be published in the journal. After a manuscript is technically edited and formatted, it will be removed from the “Just Accepted” Web site and published as an ASAP article. Note that technical editing may introduce minor changes to the manuscript text and/or graphics which could affect content, and all legal disclaimers and ethical guidelines that apply to the journal pertain. ACS cannot be held responsible for errors or consequences arising from the use of information contained in these “Just Accepted” manuscripts.

ACS Publications

is published by the American Chemical Society. 1155 Sixteenth Street N.W., Washington, DC 20036

Published by American Chemical Society. Copyright © American Chemical Society. However, no copyright claim is made to original U.S. Government works, or works produced by employees of any Commonwealth realm Crown government in the course of their duties.

Calcium-facilitated aggregation and precipitation of the uranyl peroxide nanocluster U_{60} in the presence of Na-montmorillonite

*Luke R. Sadergaski, Meena Said, and Amy E. Hixon**

Department of Civil and Environmental Engineering and Earth Sciences, University of Notre Dame, Notre Dame, IN 46556 USA

KEYWORDS: uranyl peroxide nanoclusters, montmorillonite, quartz, feldspar, alkaline cations, sorption, aggregation

ABSTRACT: The unique and diverse features of uranyl peroxide nanoclusters may contribute to the enhanced mobility of uranium in the environment. This study examines the sorption of the uranyl peroxide nanocluster $[UO_2(O_2)(OH)]_{60}^{60-}$ (U_{60}) to Na-montmorillonite (SWy-2), plagioclase (anorthite), and quartz (SiO_2) as a function of time, U_{60} concentration, and mineral concentration. SWy-2 was studied in both its untreated form as well as after two different pre-treatments, denoted partially-treated SWy-2 and fully-treated SWy-2. U_{60} was removed (~ 99%) from solution in the presence of untreated and partially-treated SWy-2. However, U_{60} was not removed from suspensions containing anorthite, quartz, or fully-treated SWy-2, even after several months. The removal of U_{60} from suspensions containing untreated SWy-2 is promoted in part by the exchange of Li^+ counterions, normally weakly associated with U_{60} in solution, for

Ca^{2+} ions naturally present in the clay. In solution, Ca^{2+} ions induce the aggregation of nanoclusters which precipitate on the surface of SWy-2. Ca-rich U_{60} aggregates associated with SWy-2 were identified and characterized by scanning electron microscopy with energy dispersive spectroscopy, Raman spectroscopy, and X-ray photoelectron spectroscopy. This research enhances our understanding of the molecular-scale processes controlling U_{60} behavior at the mineral-water interface.

INTRODUCTION

In order to design safe geologic repositories for the long-term storage of nuclear waste, it is important to understand the fate and transport of long-lived actinides such as uranium. The transport of uranium has been addressed in part by batch sorption experiments using UO_2^{2+} and various minerals under a range of geochemical conditions.[1-6] However, during the last decade, a complex family of uranyl peroxide nanoclusters has been reported.[7-8] Formation of uranyl peroxide nanoclusters may be possible under environmentally-relevant conditions, for example, at uranium ore deposits where alpha radiolysis of water may produce hydrogen peroxide in sufficient quantities for the assembly of uranium peroxide species,[9-11] yet their effect on the fate and transport of uranium is not fully understood. The sorption of uranyl peroxide nanoclusters to two common Fe(III)-bearing minerals, namely, hematite (Fe_2O_3) and goethite (FeOOH), has been reported recently.[12,13] These studies demonstrate that clusters persist in the presence of Fe(III) minerals and common alkali ions, that their sorption behavior mimics that of a discrete anionic species, and that their interactions with mineral surfaces are driven by electrostatic outer-sphere complex formation. Given that colloidal species have been shown to promote the transport of actinide species in environmental systems,[14-17] the formation of uranyl peroxide nanoclusters may represent a source term that is not currently accounted for in reactive transport models.

The uranyl peroxide nanocluster $[(UO_2)(O_2)(OH)]_{60}^{60-}$ (U_{60}) was used in this study as a model structure for the wider family of uranyl peroxide nanoclusters, which spontaneously self-assemble in solution under alkaline conditions and are several nanometers in diameter (e.g., the diameter of U_{60} is ~2.5 nm).[18,19] U_{60} is comprised of 60 compositionally identical uranyl peroxide hydroxide polyhedra, behaves like an aqueous species when dissolved in solution, and is thermodynamically stable in the absence of excess peroxide.[9,20-21] U_{60} persists in aqueous solution from pH 7.5 to 11 and the negative charge of the uranyl peroxide cage is balanced by K^+ and Li^+ both in solution and when crystallized.[18] Under the solution conditions used in the present study, Li^+ cations are not closely associated with the uranyl peroxide cage, which leaves the cage with an overall negative charge.[18,21] In the presence of excess cations, U_{60} undergoes rapid self-assembly to form blackberry-type structures, which are on the order of tens of nanometers and have been identified using transmission electron cryomicroscopy (cryo-TEM).[22] Blackberries are a particular kind of uranyl peroxide cluster aggregate that are approximately spherical, hollow, and are believed to form primarily due to counterion-mediated attractions.[23-25]

The smectite group member, montmorillonite, is a major component of the natural, geological material bentonite, which has been studied for use as an engineered barrier to ensure the immobility of long-lived nuclear waste.[26] Clay barriers will limit water flux towards waste containers and retain radionuclides because of their favorable sorption and cation exchange properties.[27] Montmorillonite is a 2:1 phyllosilicate mineral containing two tetrahedral sheets of silica on either side of a central octahedral sheet of alumina. These sheets retain a permanent negative charge (i.e., independent of pH) due to isomorphic substitution of Al(III) for Si(IV) and

Fe(II) and Mg(II) for Al(III). This generates an appreciable negative charge at the basal surface-water interface. In addition, clays also possess a variable charge because the surface charge of edge sites vary with pH.[28,29]

In this study, we examined the sorption of U_{60} to quartz, anorthite, and montmorillonite (SWy-2) as a function of mineral concentration (10 – 20 mg·mL^{-1} SWy-2), U_{60} concentration (0.5 – 2 mg·mL^{-1}), and time (20 minutes – 122 days). Batch sorption experiments were conducted to determine if clay, which is generally a strong sorbent material for contaminant species, would also be suitable to retain species such as uranyl peroxide nanoclusters; additional experiments with quartz and anorthite were conducted to determine their effect on U_{60} sorption to untreated SWy-2. We hypothesized that direct interactions between U_{60} and montmorillonite surfaces would be unfavorable due to electrostatic repulsion of the negatively charged basal plane and the negatively charged uranyl peroxide cage. However, it is conceivable that countercations associated with U_{60} might exchange for cations associated with montmorillonite and that the behavior of uranyl peroxide clusters may depend in part of the concentration and type of dissolved salts in environmental systems. This study attempts to discover if cations play a critical role in the speciation and ultimate sequestration of uranyl peroxide nanoclusters in environmental systems.

MATERIALS AND METHODS

All chemicals were commercially obtained (ACS grade) and used as received unless otherwise stated. All water used was Milli-Q quality (18.2 MΩ·cm at 25°C). Descriptions of methods used for electrospray ionization mass spectrometry (ESI-MS), Raman spectroscopy, X-ray photoelectron spectroscopy (XPS), and microfiltration can be found in the Supporting Information.

U_{60} Preparation and Characterization. U_{60} nanoclusters were synthesized according to previously published procedures[15] and characterized via single crystal X-ray diffraction using a Bruker APEXII single-crystal diffractometer with monochromated Mo Kα X-ray radiation at 100 K.

Mineral Preparation and Characterization. Anorthite was obtained from Ward's Science (mineral mined in Grass Valley, CA, USA). It was ball-milled and sieved using U.S.A. standard testing sieves to recover the 63-212 μm size fraction for use in batch sorption experiments. Quartz was obtained from the Unimin Corporation (Spruce Pine, NC) as IOTA-8 high-purity quartz and used as received. The particle size reported by Unimin Corporation is 75-300 μm.

Na-montmorillonite (SWy-2) from Crook County, Wyoming, USA was obtained from the Source Clay Repository and used in batch sorption experiments following multiple partial purification procedures: (1) 0.001 M HCl to remove soluble salts; (2) 0.03 M H_2O_2 to minimize the reducing capacity of any impurities and break-up organics associated with the clay; (3) 0.1 M NaCl rinse (four times) to produce a homo-ionic clay suspension; (4) Milli-Q water rinse to remove excess ions until a constant conductivity was achieved ($< 10\ \mu S \cdot cm^{-1}$); and (5) centrifugation to remove particles > 2 μm (3 minutes at 1000 rpm) and < 200 nm (7 minutes at 7000 rpm). Conductivity measurements were recorded using a Mettler Toledo FiveGo FG#/EL3 conductivity meter. Prepared clay was then freeze-dried using a Labconco Freezone 4.5 freeze drier. Batch sorption experiments were conducted using untreated SWy-2 to preserve its mineral integrity, partially-treated SWy-2 (i.e., steps 1 and 2 of the purification procedure), and fully-treated SWy-2 (i.e., all steps of the purification procedure). Additional mineral characterization including powder X-ray diffraction, Brunauer-Emmett-Teller (BET) surface area analysis, and zeta potential measurements can be found in the Supporting Information.

Dynamic Light Scattering (DLS). DLS was used to determine the hydrodynamic diameter (D_H) of U_{60} in aqueous solutions in the presence and absence of monovalent and divalent cations. All measurements were conducted at 25°C using a Malvern Zetasizer Nano S equipped with a He-Ne laser (λ = 633 nm) and a backscatter detector. Samples (~1 mL) were placed in disposable polystyrene cuvettes. Aliquots from 0.1 M stock solutions of NaCl, KCl, $MgCl_2$, and $CaCl_2$ were added to solutions containing 2 $mg \cdot mL^{-1}$ U_{60} until a change in the hydrodynamic diameter (indicative of aggregate formation) was detected. The U_{60} and salt stock solutions were passed through 0.2 μm polytetrafluoroethylene (PTFE) filters before DLS experiments to assure the absence of dust particles. Immediately after spiking salt solution into solutions containing U_{60}, each sample was mixed by hand and with a vortex mixer and subsequently centrifuged for 8 minutes at 9,200 rpm to remove dust and precipitates from solution. Measurements were conducted in triplicate sets of 3 runs (60 seconds each) with a 120 second equilibration time and 10 second delay between measurements. The hydrodynamic diameter (D_H) values were reported from the intensity distribution, which is based on Rayleigh scattering. The abundance of each particle was determined using the volume distribution, which is less biased toward larger particles. Further discussion is provided in the Supporting Information.

SEM-EDS analysis. Scanning electron microscopy (SEM) images were taken with a JEOL JCM-6000 Plus Neoscope Benchtop SEM at accelerating voltages from 10-15 kV. Secondary electron mode was used to examine sample morphology and compositional differences across each sample were investigated through backscatter electron (BSE) imaging. Energy dispersive X-ray spectroscopy (EDS) provided multi-element, semi-quantitative analysis through point spectra with an energy resolution of 130-150 eV. Spectra were collected at 15 kV in BSE mode using a silicon drift detector. Reacted SWy-2, unreacted SWy-2, and U_{60} aggregates (2 mg·mL^{-1} U_{60} which was intentionally precipitated from a $CaCl_2$ solution) were prepared for SEM-EDS analysis by dispersing a small quantity of material in the center of carbon tape adhered to an SEM stub.

Particle analysis was performed using ImageJ software following standard procedures.[30] Briefly, ImageJ was used to perform an automatic threshold analysis with a binary mask on select SEM images. Prior to the threshold analysis, the images were identically cropped to omit the instrument information on the bottom of the image, as it would interfere with the particle size analysis calculations. U precipitates were represented by RGB value 0 (black) while the clay background was represented by RGB value 255 (white). Using a bounding rectangle inside of each particle, ImageJ's particle analyzer calculated the height and width of each particle.

ICP-OES Analysis. Inductively coupled plasma optical emission spectroscopy (ICP-OES) was used to quantify the elemental concentrations in reactor solutions. Elemental analyses were determined using a PerkinElmer Optima 8000 DV ICP-OES instrument with 165 – 800 nm coverage and a resolution of approximately 0.01 nm for multi-elemental analysis. External calibration was used to determine the unknown elemental concentrations of U (0.2 to 20 ppm), K (0.07 to 2 ppm), Li (0.025 to 1 ppm), Fe (0.05 to 5 ppm), Ca (0.1 to 5 ppm), Mg (0.1 to 5 ppm), Na (0.1 to 5 ppm), Si (0.15 to 5 ppm) and Al (0.1 to 6 ppm). Aliquots from each reactor were dissolved in 10 mL of 5% nitric acid. An internal standard (1 ppm Y) was added to each standard, blank, and sample to monitor for instrument drift. Each dilution was measured gravimetrically, using an OHAUS model AX124/E balance with an accuracy of ±0.0001 g.

Batch Sorption Experiments. Batch sorption experiments were performed in duplicate by spiking the appropriate amount of the U_{60} stock solution into suspensions containing 235 – 470 $m^2 \cdot L^{-1}$ (10 and 20 $mg \cdot mL^{-1}$) SWy-2, 1 – 4.2 $m^2 \cdot L^{-1}$ (5 and 20 $mg \cdot mL^{-1}$) anorthite, or 100 – 500 $m^2 \cdot L^{-1}$ (29 and 147 $mg \cdot mL^{-1}$) quartz. SWy-2 suspensions were allowed to equilibrate on a rotator for 24 hours to fully hydrate the clay before the addition of U_{60}. Reactors were sampled at various time points within the time frame of minutes to months. At each time point, a 300 µL aliquot was centrifuged for 8 min at 9,200 rpm to remove clay particles ≥ 200 nm and then diluted for ICP-OES analysis.

The pH of reactors was not adjusted in order to avoid introducing species into solution which might affect the stability of U_{60}. A glass pH probe manufactured by Thermo Fisher Scientific (ORION 9103SC) was used to measure pH. The probe was placed in 0.001 M HCl for approximately ten minutes before each measurement in order to remove any soluble salts that might affect the stability of the nanoclusters.

U_{60} sorption curves were calculated as the % U removed according to eq 1, since U_{60} breaks down to $(UO_2)^{2+}$ in 5% HNO_3, where C_0 is the initial uranium concentration (ppm) and C_f is the concentration of uranium (ppm).

$$\% \, U \, Removed = \frac{C_0 - C_f}{C_0} * 100 \qquad (1)$$

RESULTS AND DISCUSSION

Aqueous-Phase Alkali and Alkaline Ion Concentrations as a Function of SWy-2 Treatment. The exchange of U_{60} into the interlayer spacing of SWy-2 is unlikely because both U_{60} and the clay sheets are negatively charged and the interlayer spacing (~1.3 nm) is smaller than the size of the uranyl peroxide cage (2.5 nm). However, we wanted to know if the countercations naturally present from the dissolution of crystals containing U_{60}, namely, K^+ and Li^+, could participate in cation exchange while leaving the uranyl peroxide cage intact and persistent in solution. We were also interested in distinguishing between the role of common alkali (i.e., Na^+ and K^+) and alkaline cations (i.e., Ca^{2+} and Mg^{2+}) in the formation of aggregates and precipitates containing U_{60}. Thus, SWy-2 was pre-treated by several means in order to gain insights into the reactivity between the concentration of salts in solution, specific exchangeable cations and U_{60}.

Uranyl peroxide nanoclusters self-assemble into larger called blackberries, which remain stable in solution over time. However, the size, shape, and rate of blackberry formation is cation-dependent.[22,23] Therefore, the concentration of alkali and alkaline ions present in solutions containing untreated and partially-treated SWy-2 could affect the aqueous speciation of U_{60}. In reactors containing 20 $mg \cdot mL^{-1}$ untreated SWy-2 we measured 3 mM Na^+, 0.1 mM K^+, 0.5 mM Mg^{2+}, and 1 mM Ca^{2+} whereas in suspensions containing 20 $mg \cdot mL^{-1}$ partially-treated SWy-2, the concentrations were approximately two times lower. The concentration of K^+ was negligible compared to the concentration of K^+ in solution naturally present from the dissolution of U_{60} crystals. The concentration of Na^+ in reactors containing 20 $mg \cdot mL^{-1}$ fully-treated SWy-2 was 6 mM, however, the concentration of K^+ and divalent cations were all below the detection limit of ICP-OES.

U_{60} Sorption as a Function of Time, U_{60} Concentration, and SWy-2 Treatment. The percentage of uranium removed from the aqueous phase of suspensions containing untreated, partially-treated, and fully-treated SWy-2 was monitored as a function of time, U_{60} concentration, and mineral concentration. The percentage of uranium removed from solution increased as a function of time in suspensions containing untreated and partially-treated SWy-2 (see Figure 1 a, b). In general, the removal was slower than sorption of the uranyl ion to natural bentonite, kaolinite, montmorillonite and the sorption of U_{60} to goethite.[1,2,13] U_{60} was removed more slowly in systems containing partially-treated SWy-2 than untreated SWy-2, which is consistent with the lower concentrations of cations we measured in solutions containing partially-treated SWy-2. Similar removal trends were observed regardless of U_{60} concentration, which implies that U_{60} was not removed from solution due to the salting-out effect (i.e., the rate of U_{60} sorption would decrease with increasing U_{60} concentration). In addition to the extent of pre-treatment, the mineral concentration played an important role in the removal of U_{60} from solution. As the untreated and partially-treated clay concentrations were increased from 10 to 20 $mg \cdot mL^{-1}$, more surface area became available, a higher concentration of cations was present, and a larger fraction of uranium was removed from solution. The removal of U_{60} from systems containing 10 $mg \cdot mL^{-1}$ partially treated SWy-2 appears to be surface-site limited, but may also be explained by the lower concentration of dissolved cations available to induce aggregation of the nanoclusters (see discussion below). U_{60} was not removed by fully-treated SWy-2 for at least four months (see Figure 1c). This was a much longer time-frame than what was needed to see removal of U_{60} in the presence of the untreated and partially treated SWy-2, which we propose is due to the removal of the exchangeable divalent cation Ca^{2+} from fully-treated SWy-2 during the pre-treatment process.

The percentage of Li^+ and K^+ (present in solution due to dissolution of U_{60} crystals) removed from solution was also monitored as a function of time (see Figure 2). Approximately half of the Li^+ was removed from solutions containing partially-treated SWy-2 within the first 30 minutes of the reaction and the amount removed remained approximately constant over the time period studied here. Similar results were obtained regardless of U_{60} concentration and in suspensions

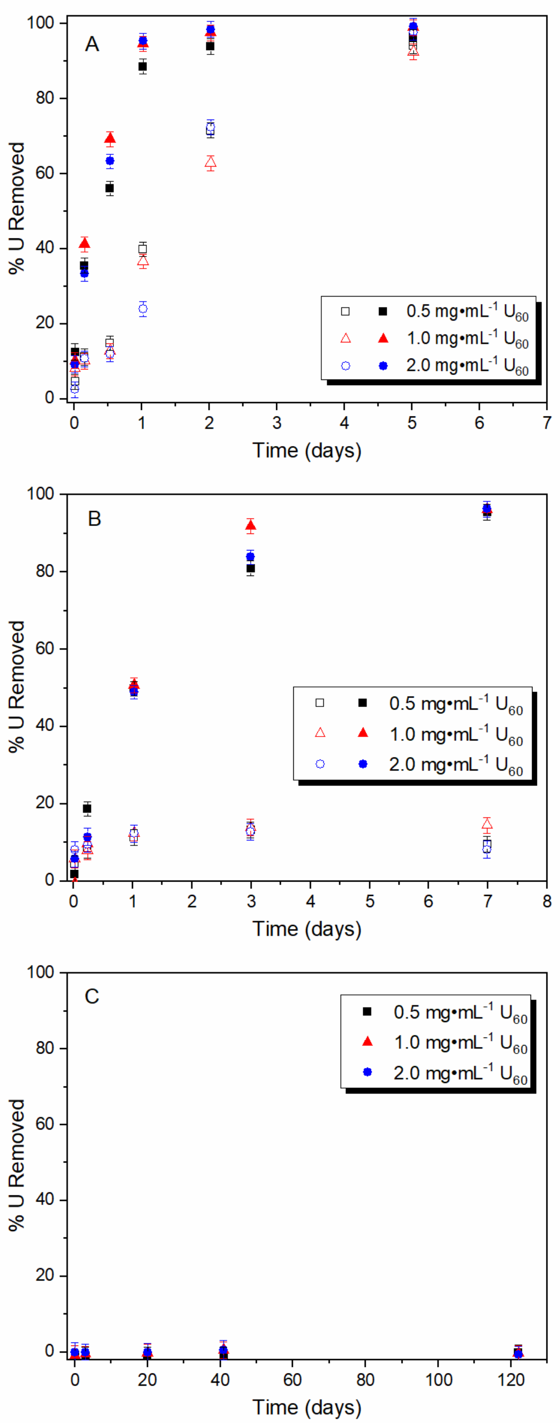

Figure 1. Percentage of uranium removed from solution as a function of time and U_{60} concentration in the presence of (A) untreated, (B) partially-treated, and (C) and fully-treated SWy-2 at pH 9.5. The pH drifted to pH 8 in the system containing fully-treated SWy-2. Note that

the x-axis scale in panel C is different than the other panels. Closed and open symbols represent 20 and 10 mg·mL^{-1} of SWy-2, respectively. Data points represent the average of duplicate samples. Error bars represent propagation of error based on the uncertainty of ICP-OES measurements and gravimetric sample preparation.

containing untreated SWy-2 (see Figure S4). These results are contrary to those observed in systems containing hematite and goethite, which showed that less Li$^+$ is removed than uranium at each time point, and is likely due to ion exchange. The fraction of K$^+$ removed was similar to that of uranium. This is expected because it is more strongly associated with the uranyl peroxide cage, however, it was not removed identically, which is different than systems containing hematite and goethite.[12,13] In the present study, a larger fraction of K$^+$ was removed from solution than uranium at early time points (i.e., 30 minutes, 5.5 hours, and 24.5 hours) and a smaller fraction was removed at later time points. This may be explained by some fraction of K$^+$, which can move in and out of the hexagonal and pentagonal windows of the uranyl peroxide cage, participating in cation exchange at early time-points. At later time-points, the remaining K$^+$ in solution could be explained by the displacement of K$^+$ inner-sphere complexes, within the hexagonal and pentagonal windows, by another cation. Even though no uranium was removed from solution in the presence of fully-treated SWy-2, K$^+$ (30%) and Li$^+$ (70%) were removed from solution before the initial sampling point at 30 minutes and remained at steady-state for at least 122 days (see Figure S16).

The concentrations of Na$^+$, Mg^{2+} and Ca^{2+}, present in solution from the SWy-2, were also monitored by ICP-OES during batch sorption experiments. In all systems containing untreated and partially-treated SWy-2, the concentration of Ca^{2+} decreased as uranium was removed from

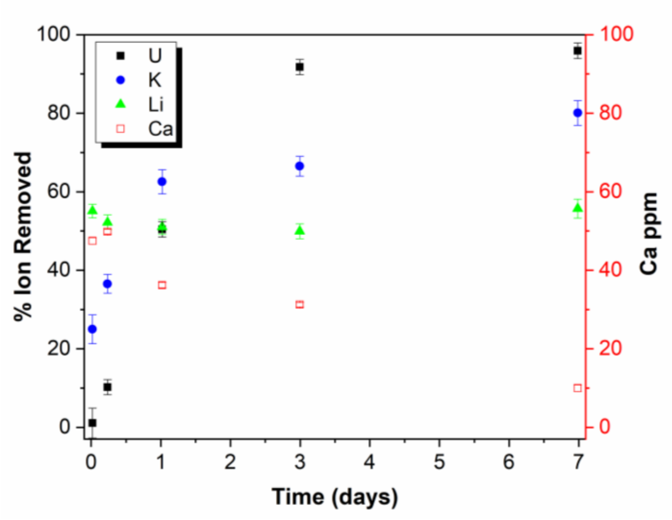

Figure 2. Percent of uranium, potassium, and lithium (present from addition of U_{60}) removed from solution as a function of time in a system containing 0.96 ± 0.01 $mg \cdot mL^{-1}$ U_{60} and 20.00 ± 0.03 $mg \cdot mL^{-1}$ partially-treated SWy-2 at pH 9.5. The concentration of Ca^{2+} in ppm (right ordinate) was measured at the same time points and is present in solution from SWy-2. Data points represent the average of duplicate samples. Error bars represent propagation of error based on the uncertainty of ICP-OES measurements and gravimetric sample preparation.

solution (see Figure 2) while the concentrations of Na^+ and Mg^{2+} did not (data not shown here). These results imply that Ca^{2+} preferentially associated with the clusters before they left solution.

The removal of Li^+ from solution is attributed to cation exchange with the exchangeable cations associated with SWy-2, which likely also contributed to the removal of U_{60} from solution. Untreated SWy-2 has a reported cation exchange capacity (CEC) of 0.85 $meq \cdot g^{-1}$ and contains both Na^+ and Ca^{2+} as exchangeable ions.[31] Each exchangeable cation is able to replace the original Li^+ cations and form linkages between uranyl peroxide cages.[22] In reactors containing 2 $mg \cdot mL^{-1}$ U_{60} and 20 $mg \cdot mL^{-1}$ untreated SWy-2, the largest amount of Li^+ exchange accounts for ~10% of the CEC. Based on the Hofmeister series,[32] it is probable that outer-sphere complexed Ca^{2+} cations were preferentially exchanged. The exchange of Li^+ for Ca^{2+} may result in one of two things: (1) the additional concentration of Ca^{2+} introduced to solution was sufficient to surpass the critical salt concentration; or (2) with Li^+ no longer charge-balancing the solution between clusters, U_{60} may be more prone to participate in charge-balancing interactions (e.g., blackberry formation) with cations such as Ca^{2+}. In either case, U_{60} would likely be removed by precipitation of large aggregates and no longer infinitely suspended in solution.

Aggregate Formation. The size distribution of U_{60} remaining in solution during batch sorption experiments was examined to determine if U_{60} was present as discrete clusters or U_{60} aggregates. The sizes of U-bearing species (determined via microfiltration) in systems containing untreated and partially-treated SWy-2 are clearly much larger than discrete U_{60} (compare Table S1 to Tables S2 and S3, respectively, in the Supporting Information) and ESI-MS revealed that U_{60} persisted in solution despite the removal of Li^+ and K^+ counterions in batch sorption experiments with fully-treated SWy-2. The exchange for Na^+ (or another cation) resulted in slight shift to a higher mass compared to U_{60} nanoclusters in solution (see Figure S5). Crystals containing U_{60} nanoclusters have not been synthesized with Na^+ as a countercation; nevertheless, Na^+ may be able to charge balance nanoclusters in solution.[9]

The major driving force for blackberry formation is counterion-mediated attraction.[24] Cations with smaller hydrated sizes are usually more effective in decreasing the charge between neighboring macroions and attracting them together.[23] Dynamic light scattering (DLS) is suitable to determine the size of particles in solution in situ and was used to monitor the aggregation of U_{60}. DLS was used to determine the minimum concentrations of alkali and alkaline ion salts required to trigger the self-assembly of U_{60} into larger structures (i.e., the critical salt concentration). An appreciable change in the hydrodynamic diameter (D_H) was observed when 2

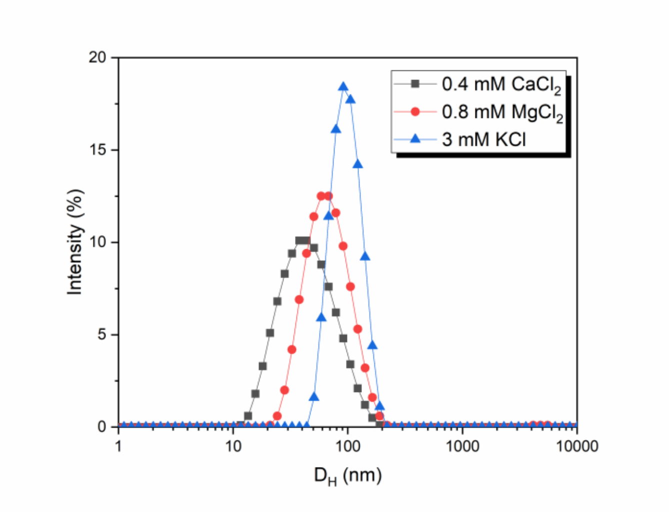

Figure 3. The average hydrodynamic diameter (D_H) of U_{60} aggregates with 0.4 mM $CaCl_2$ (39.3 nm), 0.8 mM $MgCl_2$ (60.1 nm), and 3 mM KCl (92.2 nm) after 48 hours. The average D_H of the U_{60} stock solution was 1.5 nm.

$mg{\cdot}mL^{-1}$ U_{60} was mixed with 3 mM KCl, 0.8 mM $MgCl_2$, or 0.4 mM $CaCl_2$ (see Figure 3). No appreciable change in D_H was observed, compared to pure U_{60}, below these concentrations of countercations. Only a slight change in D_H was observed in a system containing 10 mM NaCl (see Figure S6). No visible precipitation occurred at these salt concentrations.

These observations follow a normal sequence for cation interactions with polyoxometalates, which is dependent on the hydrated size of the cation (Mg^{2+} has a larger hydrated size than Ca^{2+} and Na^{+} has a larger hydrated size than K^{+}).[18] With a decrease in hydrated size, cations have a higher affinity to penetrate the electric double layer surrounding U_{60} and mediate the negative charge of the uranyl peroxide cage.[18,25] Thus, the formation of U_{60} aggregates occurred at lower concentrations for cations with smaller hydrated sizes. These results suggest that alkaline ions may follow a similar trend to the alkali ions since less Ca^{2+} is required to prompt aggregation of U_{60} than Mg^{2+}. The greater charge of divalent cations promotes the aggregation of clusters at lower concentrations (mM) than monovalent cations.[22] These results are consistent with those of Pigga et al.,[33] which describes that the selective association of the Keplerate polyoxometalate $\{Mo_{72}Fe_{30}\}$ with counterions is determined according to the valence state and hydrated size of the counterion. In accordance with Coulomb's Law, multivalent counterions interact more strongly with $\{Mo_{72}Fe_{30}\}$ than monovalent counterions.[33]

Aggregates remained in solutions containing salts for at least one month. Aggregates in the KCl system showed little fluctuation in size and volume distribution. However, the size of aggregates in the divalent systems increased slightly over time and the Mg-U_{60} aggregates were consistently larger than Ca-U_{60} aggregates, which is consistent with previous findings.[22] Overall, the sizes of these aggregates are consistent with the size of blackberries as well as secondary and tertiary structures of U_{60} observed with cryo-TEM.[22] The precipitation of U_{60} aggregates, following the addition of divalent cations to solution at concentrations above the critical salt concentration, occurred rapidly (i.e., in less than 10 minutes). However, in the case of monovalent cations such as K^+, the ripening effect took more time (i.e., days to weeks) before visible precipitation and settling of U_{60} aggregates occurred.

Given the concentration of Ca^{2+} in the SWy-2 suspensions, and the concentrations of Mg^{2+}, K^+ and Na^+ required to induce aggregation (i.e., above the concentrations in clay suspensions), aggregation induced by Ca^{2+} is likely the first step in the removal mechanism of U_{60} from solution. However, the precipitation of U_{60} from solution by a salting-out effect is not supported by the time-scales shown in the sorption curves presented in Figure 1, which occur on the order of days to weeks. Therefore, we hypothesize that the removal of U_{60} from solution cannot be solely based on aqueous phase interactions and require interactions with the clay surface.

The concentrations of cations within the electric double layer of the clay are much higher than in the bulk solution because they balance the permanent and variable negative charge of the clay sheets.[34] For example, the strongly hydrated cations Na^+ and Ca^{2+} tend to form outer-sphere surface complexes above the basal clay surface.[32] Blackberry-type structures have negatively-charged electric double layers[24] that may be attracted to the cations within the diffuse layer at the clay basal plane. Once drawn to the surface, additional blackberries will preferentially deposit themselves to form tertiary structures and large agglomerates on the surface. In essence, cations within the electric double layer generate a surface-induced salting-out effect. Therefore, we propose that the clay surface may act as a nucleation point for the formation of precipitates (species containing U_{60} aggregates).

U_{60} associated with the SWy-2 surface. Scanning electron microscopy with energy dispersive X-ray spectroscopy (SEM-EDS) was used to provide evidence for the proposed mechanism of U_{60} removal from solution as well as provide information complementary to ICP-OES results. SEM-EDS was used to confirm the presence of U-rich precipitates on the surface of reacted SWy-2 and the association of Ca with these U-rich precipitates. In backscatter electron (BSE) mode, imaging can show compositional differences based on the atomic number of the element(s) that are present. High-Z material (e.g., U) is associated with observed bright white regions whereas low-Z material (e.g., Al, Si) is associated with darker regions. As shown in Figure 4, there was clear evidence of precipitation of a high-Z material on the surface of untreated SWy-2. To confirm elemental composition, EDS point spectra were taken in regions corresponding to both high-Z and low-Z material. High U and Ca concentrations were associated with the bright white regions across the sample. The high-Z precipitate analyzed in Figure 4

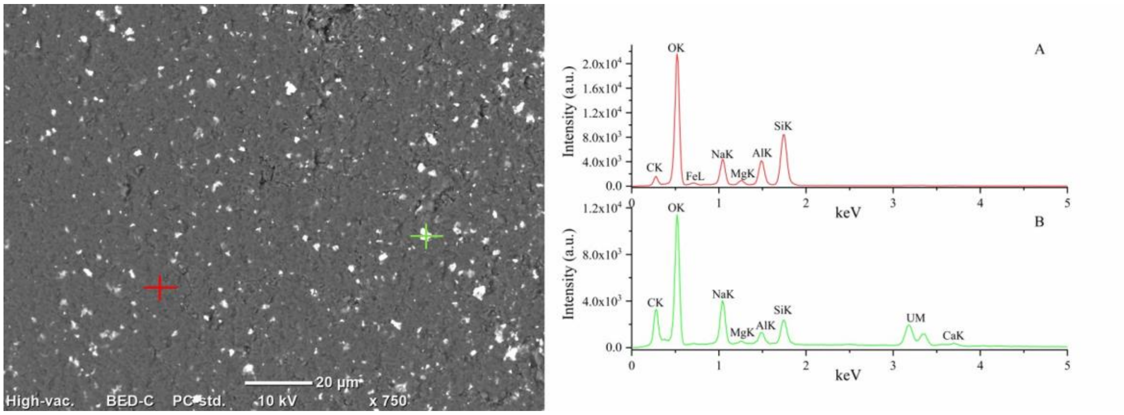

Figure 4. Scanning electron microscopy (SEM) image in backscatter electron (BSE) mode (left) and spectra using energy dispersive X-ray spectroscopy (EDS) of low-Z (A) and high-Z areas (B) showing U- and Ca-rich precipitates on the basal plane of untreated SWy-2. Sample contained 1.96 ± 0.01 mg·mL^{-1} U$_{60}$ and 20.1 ± 0.1 mg·mL^{-1} untreated SWy-2.

contained up to 67 mass % uranium and 1.5 mass % Ca; no appreciable concentration of U or Ca was measured in the low-Z region.

Additional samples were also analyzed via SEM-EDS. The shape and size of U- and Ca-rich precipitates, in a system containing 1.0 mg·mL^{-1} U$_{60}$ and 20 mg·mL^{-1} partially-treated SWy-2, were markedly similar to those shown in Figure 4 (see Figures S7 and S12). It was also confirmed with BSE imaging and EDS point spectra that U$_{60}$ was not removed from solutions containing fully-treated SWy-2 (see Figure S8), providing data that complements the ICP-OES results described above. U$_{60}$ nanoclusters were intentionally precipitated out of a CaCl$_2$ solution and analyzed via SEM-EDS to probe their morphology as a comparison to the U-rich particles described by Figure 4 (see Figure S9). The sample was made up of inhomogeneous surface features which contributed to a rough, precipitate-like quality. However, EDS showed uranium widely distributed across the material, making it difficult to discern specific morphological characteristics potentially associated with U_{60} precipitation.

Raman spectra of U_{60} crystals, U_{60} solutions, U_{60} reacted with untreated SWy-2, and U_{60} precipitated using Ca^{2+} is provided in Figure S13. The Raman signals of U_{60} solutions, which appeared at 805.4 and 843.6 cm^{-1}, were assigned to the symmetric stretching of U≡O bonds in uranyl groups and the vibrations of O–O bonds of bridging peroxo groups, respectively.[35] Raman signals at 806.1 cm^{-1} and 844.2 cm^{-1} were associated with U_{60} precipitates on the untreated SWy-2 surface and indicate that a uranyl species with a bridged peroxo group is present. Raman signals of U_{60} precipitated from a $CaCl_2$ solution, occurring at 804.7 cm^{-1} and 843.2 cm^{-1}, were almost identical to those from U_{60} crystals and U_{60} precipitated from a NaCl solution detailed in an earlier study.[12] These Raman results suggest that the precipitated species on the clay surface contains U_{60} clusters which aggregated by counterion-mediated attraction.

U 4*f* electrons were probed using XPS to determine the oxidation state of uranium on the untreated SWy-2 surface relative to crystals containing U_{60} nanoclusters. Spin-orbit interactions split the U 4*f* envelope into U $4f_{7/2}$ and U $4f_{5/2}$ peaks separated by about 10.9 eV. U(VI) satellite peaks generally appear at approximately 4 and 10 eV above these peaks.[36] Reacted powder from systems containing 2 $mg{\cdot}mL^{-1}$ U_{60} and 20 $mg{\cdot}mL^{-1}$ untreated SWy-2 were analyzed using XPS (see Figure S14). U $4f_{7/2}$ and U $4f_{5/2}$ peak positions appeared at 381.30 and 392.15 eV and U(VI) satellite positions occurred at 396.09 and 401.71 eV. These binding energies were in good agreement with those measured for U_{60} crystals. Therefore, the precipitate on the surface of SWy-2 is entirely U(VI) which indicates that any trace reductants in untreated SWy-2 do not affect the oxidation state of uranium associated with the mineral surface.

U_{60} Sorption to Anorthite and Quartz. SWy-2 is shipped as 75% smectite, 8% quartz, 16% feldspar, and 1% gypsum, mica/illite, and kaolinite/chlorite; the < 2 µm fraction contains 95% smectite, 4% quartz, and 1% feldspar, gypsum, mica/illite, and kaolinite/chlorite.[37] Therefore, batch sorption experiments were conducted with quartz and anorthite to determine if U_{60} interaction with these minerals could account for the removal of U_{60} in the presence of untreated SWy-2 sorption experiments.

There was no significant removal (i.e., < 2%) of uranium, K^+, and Li^+ from solutions containing quartz or anorthite within a 60 day time-frame (see Figure S15). The pH of these systems naturally dropped from pH 9.9 to 8, which is consistent with previous observations from systems containing U_{60} and hematite.[12] U_{60} clusters are resistant to hydrolysis, however, Li^+ ions behave like Lewis acids and are normally associated with water molecules, as opposed to the uranyl peroxide cage.[18] Thus, the drop in pH may be attributed to the hydrolysis chemical reaction between hydrated Li^+ ions and water. ESI-MS and microfiltration demonstrated that U_{60} persisted and remained intact, at a size consistent with discrete U_{60}, throughout batch sorption experiments with anorthite and quartz (data not shown). The absence of U_{60} sorption is likely due to electrostatic repulsion of the negatively-charged U_{60} cage by the negatively-charged mineral surfaces since the suspension pH is well above the PZC/IEP of each mineral.[38] This suggests that countercations associated with uranyl peroxide clusters are insufficient to mediate the interactions between the negatively charged uranyl peroxide cage and the negatively charged surface.

Anorthite, the calcium endmember of the plagioclase series within the feldspar group, was used for these studies because experiments with untreated SWy-2 indicated that calcium played an important role in U_{60} sorption. Because electrostatics govern U_{60} sorption interactions[13] and feldspars are generally characterized by low PZCs[38] we would not expect different results if a more common feldspar, such as albite, was used instead of anorthite.

Environmental Implications. Uranyl peroxide nanoclusters may not be effectively retained by a large portion of reactive surface sites available in relevant geochemical systems. Quartz, with chemical formula SiO_2, is the second most abundant mineral, behind feldspar, in the Earth's crust. Electrostatic repulsion of the negatively charged uranyl peroxide nanoclusters inhibits their interactions with quartz and anorthite. On the contrary, U(VI) readily forms sorption complexes with these minerals.[4-6] Feldspar and quartz are major constituents of granitic materials, which have been proposed geologic hosts for nuclear repositories. However, the results from this study suggest that they may not be useful in retaining species such as uranyl peroxide nanoclusters.[4]

It is unlikely that U_{60} is interacting via an inner-sphere sorption complex with montmorillonite. This is due in part to the unreactive '-yl' oxygens which truncate the uranyl peroxide cage, full coordination of uranium in the equatorial plane, and the relatively low charge/radius density of U_{60}. There are three apparent types of clay surfaces: (1) external basal surfaces, (2) clay edges, and (3) interlayer basal surfaces. Given the negatively charged clay sheets, variable negative charge at the pH these experiments were conducted under,[28,29] and the fact that U_{60} clusters are larger than the interlayer d-spacing (~1.3 nm) of SWy-2, we would not expect uranyl peroxide nanoclusters to interact with the clay. However, Li^+ and K^+ countercations may undergo cation exchange for cations in the interlayer space and relatively minute concentrations of alkali and alkaline ions trigger the formation of U_{60} aggregates. U_{60} aggregates may be relatively persistent in solution but behave more like colloidal species than soluble macroions given their large size. They may be more attracted to the greater concentration of cations within the electrical double layer at the mineral surface relative to the bulk solution than discrete nanoclusters.

Although cations such as Ca^{2+} enhance the mobility of discrete U(VI) through the formation of neutrally-charged ternary species (e.g., $Ca_2UO_2(CO_3)_3$ (aq)),[5,6] it appears that low concentrations of Ca^{2+} may be responsible for immobilizing U_{60} in the form of precipitates. Therefore, the fate and transport of uranyl peroxide clusters in environmental systems may be considerably dependent on the concentration of naturally abundant cations such as Ca^{2+} and further research in this area is warranted.

ASSOCIATED CONTENT

Supporting Information. The following files are available free of charge.

Extended materials and methods section, pXRD diffraction patterns of untreated minerals, and additional experimental results (e.g., ESI-MS, DLS, SEM, Raman, and XPS) (MS Word)

AUTHOR INFORMATION

Corresponding Author

*Telephone: +1 (574) 631-1872; E-mail address: ahixon@nd.edu.

Author Contributions

The manuscript was written through contributions of all authors. All authors have given approval to the final version of the manuscript.

Funding Sources

This material is based on work supported as part of the Materials Science of Actinides, an Energy Frontier Research Center funded by the U.S. Department of Energy, Office of Science, Office of Basic Energy Sciences under award number DE-SC0001089. Student funding was provided in part by the CEST Bayer pre-doctoral research fellowship (L. R. Sadergaski) and the Arthur J. Schmitt Leadership fellowship in Science and Engineering (M. Said).

Notes

The authors declare no competing financial interest.

ACKNOWLEDGMENT

The authors thank Mr. Samuel N. Perry and Ms. Rebecca A. Carter for help with the TOC image. The following centers and facilities at the University of Notre Dame provided access to instrumentation used in this research study: the Center for Environmental Science and Technology (CEST) (BET, ICP-OES, zeta potential), the Mass Spectrometry and Proteomics Facility (ESI-MS), and the Center for Sustainable Energy's Materials Characterization Facility (powder X-ray diffraction, Raman spectroscopy).

REFERENCES

(1) Bachmaf, S.; Merkel, B. J. Sorption of uranium(VI) at the clay mineral-water interface. *Environ. Earth Sci.* **2011**, *63* (5), 925-934; DOI 10.1007/s12665-010-0761-6.

(2) Hu, W.; Lu, S.; Song, W.; Chen, T.; Hayat, T.; Alsaedi, N. S.; Chen, C.; Liu, H. Competitive adsorption of U(VI) and Co(II) on montmorillonite: A batch and spectroscopic approach. *Appl. Clay Sci.* **2018**, *157*, 121–129; DOI 10.1016/j.clay.2018.02.030.

(3) Um, W.; Serne, R. J.; Brown, C. F.; Rod, K. A. Uranium(VI) Sorption on Iron Oxides in Hanford Site Sediment: Application of a Surface Complexation Model. *Appl. Geochem.* **2008**, *23* (9), 2649–2657; DOI 10.1016/j.apgeochem.2008.05.013.

(4) Gao, X.; Bi, M. Shi, K.; Chai, Z., Wu, W. Sorption characteristic of uranium(VI) onto K-feldspar. *Appl. Radiat. Isot.* **2017**, *128*, 311-317; DOI 10.1016/j.apradiso.2017.07.041.

(5) Richter, C.; Müller, K.; Drobot, B.; Steudtner, R.; Grossmann, K.; Stockmann, M.; Brendler, V. Macroscopic and spectroscopic characterization of uranium(VI) sorption onto orthoclase and muscovite and the influence of competing Ca^{2+}. *Geochim. Cosmochim. Acta* 2016, *189*, 143-157; DOI 10.1016/j.gca.2016.05.045.

(6) Fox, P. M.; Davis, J. A.; Zachara, J. M. The effect of calcium on aqueous uranium(VI) speciation and adsorption to ferrihydrite and quartz. *Geochim. Cosmochim. Acta* **2006**, *70* (6), 1379-1387; DOI 10.1016/j.gca.2005.11.027.

(7) Burns, P. C.; Nyman, M. Captivation with Encapsulation: A Dozen Years of Exploring Uranyl Peroxide Capsules. *Dalton Trans.* **2018**, *47* (17), 5916–5927; DOI 10.1039/C7DT04245K.

(8) Qiu, J.; Burns, P. C. Clusters of Actinides with Oxide, Peroxide, or Hydroxide Bridges. *Chem. Rev.* **2013**, *113* (2), 1097–1120; DOI 10.1021/cr300159x.

(9) Armstrong, C. R.; Nyman, M.; Shvareva, T.; Sigmon, G. E.; Burns, P. C.; Navrotsky, A. Uranyl peroxide enhanced nuclear fuel corrosion in seawater. *Proc. Natl. Acad. Sci. U. S. A.* **2012**, *109* (6), 1874–1877; DOI 10.1073/pnas.1119758109.

(10) Kubatko, K.-A. H.; Helean, K. B.; Navrotsky, A.; Burns, P. C. Stability of Peroxide-Containing Uranyl Minerals. *Science* **2003**, *302* (5648), 1191–1193; DOI 10.1126/science.1090259

(11) Burns, P. C.; Ewing, R. C.; Navrotsky, A. Nuclear Fuel in a Reactor Accident. *Science* **2012**, *335* (6073), 1184–1188; DOI 10.1126/science.1211285.

(12) Sadergaski, L. R.; Stoxen, W.; Hixon, A. E. Uranyl Peroxide Nanocluster (U_{60}) Persistence and Sorption in the Presence of Hematite. *Environ. Sci. Technol.* **2018**, *52* (5), 3304-3311; DOI 10.1021/acs.est.7b06510.

(13) Sadergaski, L. R.; Hixon, A. E. Kinetics of Uranyl Peroxide Nanocluster (U_{60}) Sorption to Goethite. *Environ. Sci. Technol.* **2018**, *52* (17), 9818-9826; DOI 10.1021/acs.est.8b02716.

(14) Walther, C.; Denecke, M. A. Actinide Colloids and Particles of Environmental Concern. *Chem. Rev.* **2013**, *113* (2), 995-1015; DOI 10.1021/cr300343c.

(15) Novikov, A. P.; Kalmykov, S. N.; Utsunomiya, S.; Ewing, R. C.; Horreard, F.; Merkulov, A.; Clark, S. B.; Tkachev, V. V.; Myasoedov, B. F. Colloid Transport of Plutonium in the Far-Field of the Mayak Production Association, Russia. *Science*, **2006**, *314* (5799), 638-641; DOI 10.1126/science.1131307.

(16) Santschi, P. H.; Roberts, K. A.; and Guo, L. Organic Nature of Colloidal Actinides Transported in Surface Water Environments. *Environ. Sci. Technol.* **2002**, *36* (17), 3711–3719; DOI 10.1021/es0112588.

(17) Kersting, A. B.; Efurd, D. W.; Finnegan, D. L.; Rokop, D. J.; Smith, D. K.; Thompson, J. L. Migration of plutonium in group water at the Nevada Test Site. *Nature*, **1999**, *397*, 56–59; DOI 10.1038/16231.

(18) Peruski, K. M.; Bernales, V.; Dembowski, M.; Lobeck, K. L.; Pellegrini, K. L.; Sigmon, G. E.; Hickam, S. Wallace, C. M.; Szymanowski, J. E. S.; Balboni, E.; Gagliardi, L.; Burns, P. C. Uranyl Peroxide Cage Cluster Solubility in water and the Role of the Electrical Double Layer. *Inorg. Chem.* **2017**, *56* (3), 1333-1339; DOI 10.1021/acs.inorgchem.6b02435.

(19) Sigmon, G. E.; Unruh, D. K.; Ling, J.; Weaver, B.; Ward, M.; Pressprich, L.; Simonetti, A.; Burns, P. C. Symmetry versus Minimal Pentagonal Adjacencies in Uranium-Based Polyoxometalate Fullerene Topologies. *Angew. Chem. Int. Ed.* **2009**, *48* (15), 2737-2740; DOI 10.1002/anie.200805870.

(20) Olds, T. A.; Dembowski, M.; Wang, X.; Hoffman, C. Alam, T. M.; Hickam, S.; Pellegrini, K. L.; He, J.; Burns, P. C. Single-Crystal Time-of-Flight Neutron Diffraction and Magic-Angle-Spinning NMR spectroscopy Resolve the Structure of ^{1}H and ^{7}Li Dynamics of the Uranyl Peroxide Nanocluster U_{60}. *Inorg. Chem.* **2017**, *56* (16), 9679-9683; DOI 10.1021/acs.inorgchem.7b01174.

(21) Flynn, S. L.; Szymanowski, J. E. S.; Gao, Y.; Liu, T.; Burns, P. C.; Fein, J. B. Experimental measurements of U60 nanocluster stability in aqueous solution. *Geochim. Cosmochim. Acta* **2015**, *156*, 94-105; DOI 10.1016/j.gca.2015.02.021.

(22) Soltis, J. A.; Wallace, C. M.; Penn, R. L.; Burns, P. C. Cation-Dependent Hierarchical Assembly of U60 Nanoclusters into Macro-Ion Assemblies Imaged via Cryogenic Transmission Electron Microscopy. *J. Am. Chem. Soc.* **2016**, *138* (1), 191-198; DOI 10.1021/jacs.5b09802.

(23) Gao, Y.; Haso, F.; Szymanowski, J. E. S.; Zhou, J.; Hu, L.; Burns, P. C.; Liu, T. Selective Permeability of Uranyl Peroxide Nanocages to Different Alkali Ions: Influences from Surface Pores and Hydration Shells. *Chem. Eur. J.* **2015**, *21* (51), 18785-18790; DOI 10.1002/chem.201503773.

(24) Liu, T. Hydrophilic Macroionic Solutions: What Happens When Soluble Ions Reach the Size of Nanometer Scale? *Langmuir* **2010**, *26* (12), 9202-9213; DOI 10.1021/la902917q.

(25) Pigga, J. M.; Kistler, M. L.; Shew, C-Y.; Antonio, M. R.; Liu, T. Counterion Distribution around Hydrophilic Molecular Macroanions: The Source of the Attractive Force in Self-Assembly. *Angew. Chem.* **2009**, *121* (35), 6660-6664; DOI 10.1002/ange.200902050.

(26) Sellin, P.; Leupin, O. X. THE USE OF CLAY AS AN ENGINEERED BARRIER IN RADIOACTIVE MANAGEMENT – A REVIEW *Clays Clay Miner.* **2013**, *61* (6), 477-498; DOI 10.1346/CCMN.2013.0610601.

(27) Zavarin, M.; Powell, B. A.; Bourbin, M.; Zhao, P.; Kersting, A. B. Np(V) and Pu(V) Ion Exchange and Surface-Mediated Reduction Mechanisms on Montmorillonite. *Environ. Sci. Technol.* **2012**, *46* (5), 2692-2698; DOI 10.1021/es203505g.

(28) Pecini, E. M.; Avena, M. J. Measuring the Isoelectric Point of the Edges of Clay Mineral Particles: The Case of Montmorillonite. *Langmuir* **2013**, *29* (48), 14926-14934; DOI 10.1021/la403384g.

(29) Liu, X.; Lu, X.; Sprik, M.; Cheng, J.; Meijer, E. J.; Wang, R. Acidity of edge surface sites of montmorillonite and kaolinite. *Geochim. Cosmochim. Acta* **2013**, *117*, 180-190; DOI 10.1016/j.gca.2013.04.008.

(30) Ferreira, T.; Rasband, W. S. *ImageJ User Guide — IJ 1.46r*; https://imagej.nih.gov/ij/docs/guide/.

(31) Borden, D.; Giese, R. F. BASELINE STUDIES OF THE CLAY MINERALS SOCIETY SOURCE CLAYS: CATION EXCHANGE CAPACITY MEASUREMENT BY THE AMMONIA-ELECTRODE METHOD. *Clays Clay Miner.* **2001**, *49* (5), 444-445; DOI 10.1346/CCMN.2001.0490510.

(32) Underwood, T.; Erastova, V. and Greenwell, H. C. ION ADSORPTION AT CLAY-MINERAL SURFACES: THE HOFMEISTER SERIES FOR HYDRATED SMECTITE MINERALS *Clays Clay Miner.* **2016**, *64* (4) 472-487; DOI 10.1346/CCMN.2016.0640310.

(33) Pigga, J. M.; Teprovich, J. A.; Flowers, R. A.; Antonio, M. R.; Liu, T. Selective Monovalent Cation Association and Exchange around Keplerate Polyoxometalate Macroions in Dilute Aqueous Solutions. *Langmuir*, **2010**, *26* (12), 9449-9456; DOI 10.1021/la100467p.

(34) Segad, M.; Jonsson, B.; Akesson, T.; Cabane, B. Ca/Na Montmorillonite: Structure, Forces and Swelling Properties. *Langmuir* **2010**, *26* (8), 5782-5790; DOI 10.1021/la9036293.

(35) McGrail, B. T.; Sigmon, G. E.; Jouffret, L. J.; Andrews, C. R.; Burns, P. C. Raman Spectroscopic and ESI-MS Characterization of Uranyl Peroxide Cage Clusters. *Inorg. Chem.* **2014**, *53* (3), 1562-1569; DOI 10.1021/ic402570b.

(36) Schindler, M.; Hawthorne, F. C.; Freund, M. S.; Burns, P. C. XPS spectra of uranyl minerals and synthetic uranyl compounds. I: The U 4f spectrum. *Geochim. Cosmochim. Acta* **2009**, *73* (9), 2471-2487; DOI 10.1016/j.gca.2008.10.042.

(37) Chipera, S. J.; Bish, D. L. BASELINE STUDIES OF THE CLAY MINERALS SOCIETY SOURCE CLAYS: POWDER X-RAY DIFFRACTION ANALYSIS. *Clays Clay Miner.* **2001**, *49* (5), 398-409; DOI 10.1346/CCMN.2001.0490507.

(38) Sverjensky, D. A. Zero-point-of-charge prediction from crystal chemistry and solvation theory. *Geochim. Cosmochim. Acta* **1994**, *58* (14), 3123-3129; DOI 10.1016/0016-7037(94)90184-8.

(39) Shirley, D. A. High-Resolution X-Ray Photoemission Spectrum of the Valence Bands of Gold. *Phys. Rev. B* **1972**, *5* (12), 4709–4714; DOI 10.1103/PhysRevB.5.4709.

(40) Dogan, A. U.; Dogan, M.; Onal, M.; Sarikaya, Y.; Aburub, A.; Wurster, D. E. BASELINE STUDIES OF THE CLAY MINERALS SOCIETY SOURCE CLAYS: SPECIFIC SURFACE AREA BY THE BRUNAUER EMMET TELLER (BET) METHOD. *Clays Clay Miner.* **2006**, *54* (1), 62-66; DOI 10.1346/CCMN.2006.0540108.

(41) Brantley, S. L.; Mellott, N. P. Surface area and porosity of primary silicate minerals. *Am. Mineral.* **2000**, *85* (11-12), 1767-1783; DOI 10.2138/am-2000-11-1220.

(42) Malvern Instruments. Size Theory. *Zetasizer Nano User Manual*. Worcestershire United Kingdom, 2010, MAN0317-5.0, pages 13-1-13-5.

TOC GRAPHIC